

Vibrational study of various crystalline phases of thallium dihydrogen phosphate TlH_2PO_4 and its deuterated analog TlD_2PO_4

Bernadette Pasquier¹, Nicole Le Calvé, Samira Al Homsî-Teiar and François Fillaux

*Laboratoire de Spectrochimie Infrarouge et Raman, Centre National de la Recherche Scientifique,
2 rue Henri Dunant, 94320 Thiais, France*

Received 22 October 1992

Vibrational spectra of thallium dihydrogen TlH_2PO_4 and dideuterium TlD_2PO_4 phosphates have been obtained in the 4000–10 cm^{-1} region as a function of temperature between 5 and 460 K. FT infrared absorption, Raman and inelastic neutron scattering spectra of polycrystalline samples are reported. Single crystals of TlH_2PO_4 were studied by reflection in the infrared and Raman spectroscopies. The spectra reveal two structural first-order phase transitions at ≈ 357 and ≈ 230 K for TlH_2PO_4 and ≈ 400 and ≈ 350 K for TlD_2PO_4 . In addition there is another transition at 127 K for TlD_2PO_4 . This latter one is an order–order type transition while the other two correspond to successive ordering of the O.H...O hydrogen bonds and to orientation of the PO_4 tetrahedra. The three hydrogen bonds and the Tl^+ crystalline sites appear to be more similar in TlD_2PO_4 than in TlH_2PO_4 . The sequences of phase transitions in both compounds are compared. TlH_2PO_4 may become ferroelectric at low temperature. The unusual behaviour of TlH_2PO_4 at low temperature (6 K) which exists as a highly disordered phase and gives an ordered phase at higher temperature may be related to the high deformability of the Tl^+ ions.

1. Introduction

Thallium dihydrogen phosphate TlH_2PO_4 (TDP) belongs to the KH_2PO_4 (KDP) family. In this family, neutron diffraction [1] shows that the protons or deuterons are disordered between two equivalent positions along the O.H...O hydrogen bonds above the temperature (T_c) of the paraelectric–ferroelectric transition. These protons become ordered below this temperature. The large increase of T_c upon deuteration was explained by proton (or deuteron) tunnelling [2]. The collective mode of the proton, expected from the Slater's rules, should be coupled with some of the translational $\text{M}^+ - \text{PO}_4^-$ optical modes inducing a soft mode behaviour. An overdamped mode above T_c and an underdamped one below T_c have been assigned to the soft mode [2]. Alternatively it has been proposed that the phase transition could be of the order–disorder type [3] with respect to the H_2PO_4 dipoles. This suggestion is based upon the ob-

servation [4] above T_c of PO_4 Raman lines which are forbidden for the S_4 site-symmetry given by neutron and by X-ray diffractions [5]. Only C_2 or C_1 sites-symmetries [4] were consistent with the observed Raman lines. The features at low frequency were then assigned to a relaxational (central) mode. The isotopic effect on T_c is proposed to be due to geometric distortion, especially expansion of the hydrogen bonds. In KDP-type crystals this expansion has been explained without invoking proton tunnelling [6,7]. Two different contributions have been proposed: a strong correlation between the hydrogen (deuterium) potential function and the O...O distances and different amplitudes for the hydrogen and deuterium fluctuations [7]. Recently, neutron diffraction measurements [8] on PbHPO_4 under hydrostatic pressure revealed that when the distances between the two locations of the H/D atom in the hydrogen bond become identical for the hydrogen/deuterium compounds then T_c^D and T_c^H are similar.

Vibrational studies of TDP and of its deuterated analog TlD_2PO_4 (DTDP) were undertaken to ob-

¹ To whom correspondence should be addressed.

serve these different effects. Vibrational spectroscopy is unique to characterizing site-symmetry, variations of the interatomic distances, specially in the case of hydrogen, and proton dynamics.

TDP is quasi-isomorphous with CsH_2PO_4 [9]. The H_2PO_4^- ions are linked by three different strong hydrogen bonds, one of them being the shortest ever reported for the KDP type crystals. Phase transitions were observed near 230 K (T_c) [10,11] and 357 K (T_p) [12,13] for TDP. The first transition is related to the disordering of the chain of the two shorter hydrogen bonds [14]. For the deuterated derivative TlD_2PO_4 (DTDP) two transitions have been reported: a first one near 350 K (T_c) [15,16] related to that at 230 K in TDP with $T_c^D = 1.5T_c^H$ and a second one of the order–order type at 127 K (T_d) [10,11] which has apparently no analog in TDP. Above T_c , TDP and DTDP are paraelectric [16]. Below T_c , DTDP is antiferroelectric like $\text{NH}_4\text{H}_2\text{PO}_4$, while such property could not be found in TDP [16]. However below T_c [17] this compound does not appear ferroelectric either. The high temperature phase transition (T_p) transforms the paraelectric–ferroelastic phase into a paraelectric–paraelastic phase [18].

The existence of a very short hydrogen bond ($R_{\text{O-O}}=0.243$ nm) is a specific feature of the thallium analog of the KDP family. This may be of importance for the order–disorder transitions and relaxation phenomena. In addition the large atomic mass of the Tl^+ cation decreases considerably the $\text{M}^+-\text{H}_2\text{PO}_4^-$ translational mode frequencies and should modify the coupling with an eventual collective mode of the protons.

Previous vibrational studies of the different phases of TDP and DTDP [15,19] do not provide a detailed analysis of the dynamics around T_c . We investigated the 10–4000 cm^{-1} range at various temperatures from melting to 5 K [20]. The inelastic neutron-scattering spectrum of TDP at 20 K is presented. The structure and dynamics of the various phases are discussed in this paper.

2. Experimental

The TDP compound was obtained from an aqueous solution of Tl_2CO_3 and H_3PO_4 with an excess of acid.

Needle-shaped crystals of TDP were precipitated by addition of ethanol. The deuterated derivative DTDP was obtained by exchange with D_2O . The deuterium concentration was better than 98 at%. This could be reduced to 90 at% in Nujol mull. For polarized Raman study, a single crystal of TDP was grown by slow evaporation from an aqueous solution at 313 K. The crystal showed large twinned domains. A single domain ($5 \times 5 \times 4$ mm^3) was cut with its edges parallel to the crystallographic axes, which are closed to the indicatrix axes. The binary axis, b , was identified by X-ray diffraction. The a and c directions were controlled by infrared dichroism. For the reflection in the infrared small single crystal plates (5×5 mm^2) of TDP were obtained by slow evaporation of an aqueous solution at room temperature. X-ray diffraction showed that the developed face is parallel to the (100) plane.

The Raman spectra were recorded on a triple monochromator RTI Dilor spectrometer. The 514.5 nm exciting-line of a Spectra Physics ionised argon laser was used. The spectral resolution was better than 1 cm^{-1} for the low-temperature spectra. The samples were sealed in glass tubes under helium atmosphere for spectra at low temperature.

The absorption spectra in the infrared of crystalline powder mullied in Nujol or Fluorolube were recorded on a Perkin-Elmer 983 spectrometer in the mid-infrared region and on a Bruker FTIR 113V spectrometer in the mid- and far-infrared regions. For the studies below 200 cm^{-1} , a bolometer detector was used. The reflection measurements in the infrared of single crystals were also obtained on the Bruker spectrometer. Transverse optical frequencies were calculated with a fitting procedure of the dielectric response using four parameters [21].

Conventional cryostats and heating cells were used for measurements in the 5–460 K range. The temperature of the sample holder was measured within ± 1 K. However, the actual temperature of the sample at the light-beam impact could be higher by a few kelvin.

The inelastic neutron-scattering measurements of a polycrystalline sample of TDP were carried out on the TFXA spectrometer at the ISIS pulsed neutron source (Rutherford Appleton Laboratory, UK). The powder was wrapped into an aluminum foil which was mounted into a liquid helium cryostat. The spectra were converted from counts per channel to the

scattering function $S(Q, w)$ per energy transfer (cm^{-1}) by standard programs.

3. Crystallographic data

The paraelectric phases of TDP [17,22] and of DTDP [23] belong to the monoclinic system, $P2_1/a$ space group, with four formula units in the primitive cell. The site symmetry is C_1 for the PO_4 groups. The O...O distances of the three hydrogen bonds of TDP obtained from neutron-diffraction measurements at room temperature [22] are 0.243 nm (HB_1), 0.247 nm (HB_2) and 0.250 nm (HB_3). The shortest hydrogen bonds HB_1 and HB_2 are alternated in the chains parallel to the c crystallographic axis (fig. 1) and are

centrosymmetric. Their O...O distances [6] suggest that protons in HB_2 should be crystallographically disordered between two sites whilst protons in the HB_1 could be either on the centre of inversion or disordered. A second type of hydrogen bonded chains parallel to the binary b crystal axis cross-link the first ones. In these chains the protons are ordered above T_c .

X-ray diffraction measurements below T_c [23] reveal a doubling of the smaller monoclinic cell in the (001) plane relatively to the paraelectric cell above T_c for both TDP and DTDP.

Above T_p , TDP is orthorhombic, D_{2h} space group, with four formula units in the primitive cell [12,18,24]. Though the atomic coordinates are not known, the site-symmetry for the PO_4 groups must

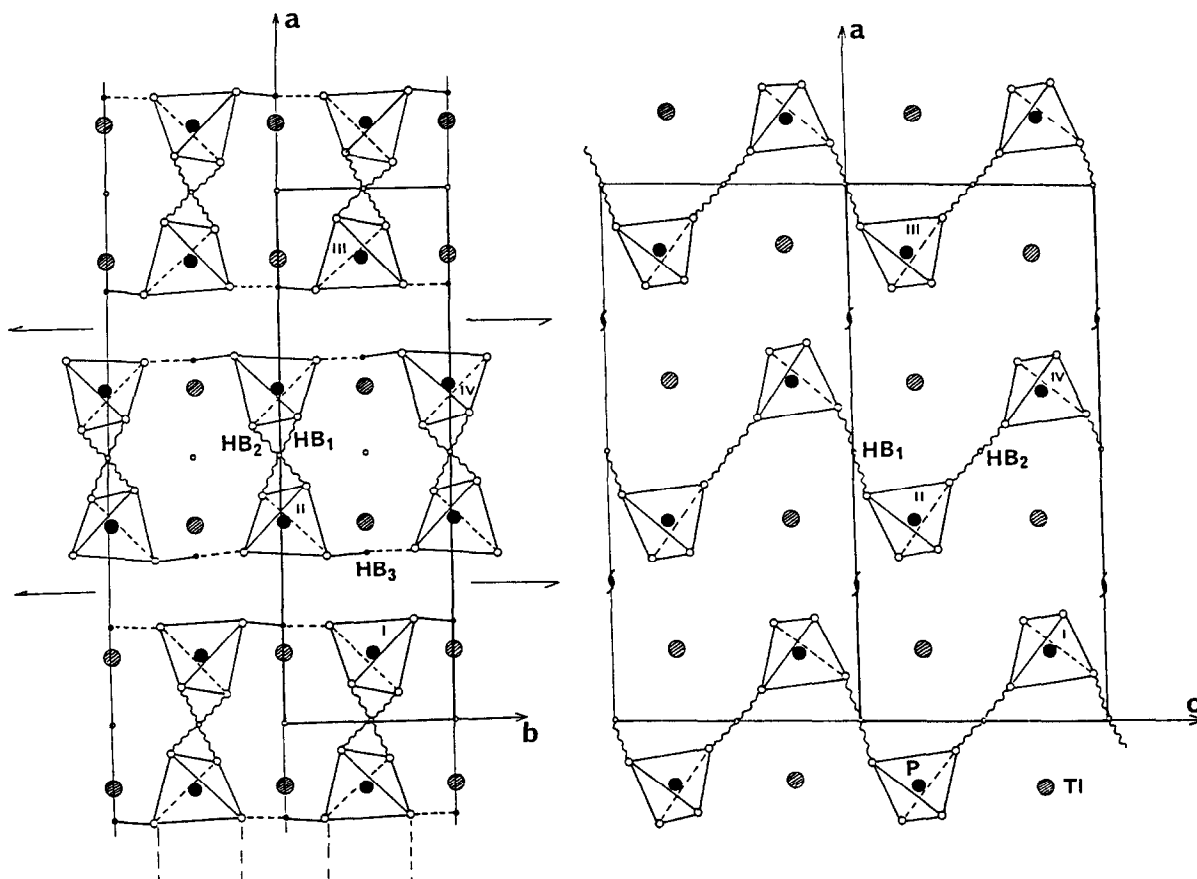


Fig. 1. Crystal structure of TIH_2PO_4 at 300 K, from neutron-diffraction data in ref. [22]. Hydrogen bonds: HB_1 (0.243 nm), HB_2 (0.247 nm), HB_3 (0.250 nm).

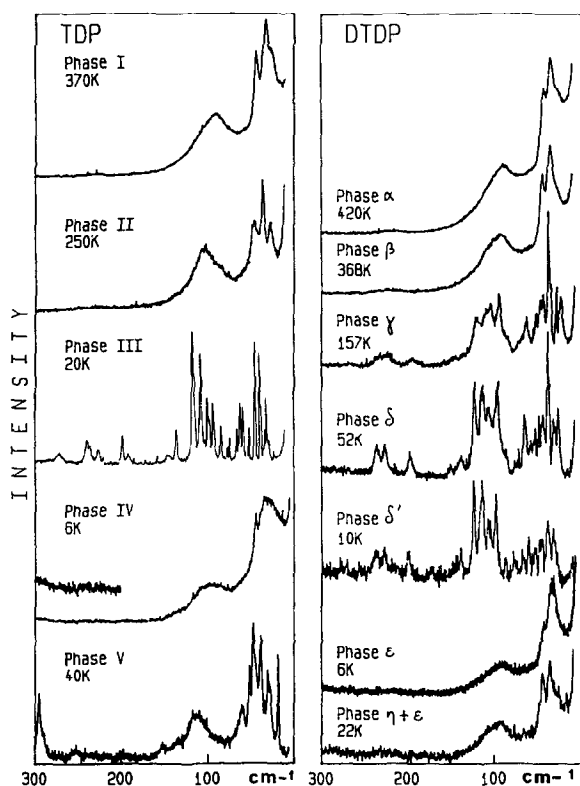


Fig. 2. Low-frequency Raman spectra of various phases of TlH_2PO_4 (TDP) and TlD_2PO_4 (DTDP).

be C_2 or C_s . The disordering of the HB_3 hydrogen bonds has been proposed [18].

In the case of DTDP the monoclinic lattice is quasi-orthorhombic above and below T_c . Even a D_{2h} space group has been proposed for the antiferroelectric phase [25]. However, this is not correct if the paraelectric phase is really monoclinic [23].

4. Phase diagram of TDP and DTDP

A superficial analysis of Raman and infrared spectra at various temperatures (figs. 2–4) allows to establish a phase diagram at atmospheric pressure for both TDP and DTDP (fig. 5). Due to the structural differences between TDP and DTDP, both systems of phases are labelled differently.

In the case of TDP five phases denoted I–V were identified between the melting point and 5 K. In the

case of the deuterated analog five main phases, α , β , γ , δ , δ' were also characterized. Two other phases ϵ and η could be observed in the latter compound.

The I–II–III and α – β – γ – δ – δ' sequences are reversible and independent of the thermal history of the crystal. In the case of TDP, the spectra of phase III at low temperature show a great number of narrow lines. Most of them are due to a progressive splitting of the bands observed at room temperature (figs. 3 and 4). The possibility of an intermediate structural phase transition near 130 K cannot be excluded, since the splitting of the internal mode near 900 cm^{-1} and of some external bands (fig. 3) is observed only below this temperature. The phase I is characterized essentially by an intense infrared absorption observed near 800 cm^{-1} above T_p (fig. 4). In the case of DTDP the phases β above T_c , γ above T_d and δ below T_d , which have already been evidenced [10,11,16], are clearly identified on the curves shown in fig. 3. Besides, two new phases are observed. The low-frequency Raman spectra of the phase δ' show less bands than in the phase δ (fig. 3). In particular the band near 25 cm^{-1} disappears below 30 K. The phase α presents a characteristic infrared spectrum above 400 K (fig. 4).

Fig. 2 shows that at low temperature new phase sequences occur for TDP (III–IV–V) and DTDP (δ – ϵ – η). In the case of DTDP, the disordered phase ϵ was obtained with a deuterated compound with about 90 at%. The phases IV and ϵ are characterized by an important broadening of all the Raman lines. The bandwidths are similar to those in the disordered phases I and α . The phases IV and ϵ are not stable. They convert easily into new ordered phases V and $\eta(+\epsilon)$, respectively (figs. 2 and 6). Their spectra show again many narrow lines, especially a new strong Raman band near 18 cm^{-1} . Upon heating these latter phases turn into the phases III and δ , respectively. The transitions IV–V–III and ϵ – η – δ are of the first order. The coexistence of these phases is observed. The occurrence of the phase IV could be related to a previously reported thermal accident in the specific heat curve versus temperature below 40 K [15]. However, this was not observed on a single crystal [10,11]. Moreover, it appears that annealed samples never give this phase. This disordered state at low temperature is thus likely to originate from crystal defects.

Finally, the liquid state can be obtained without

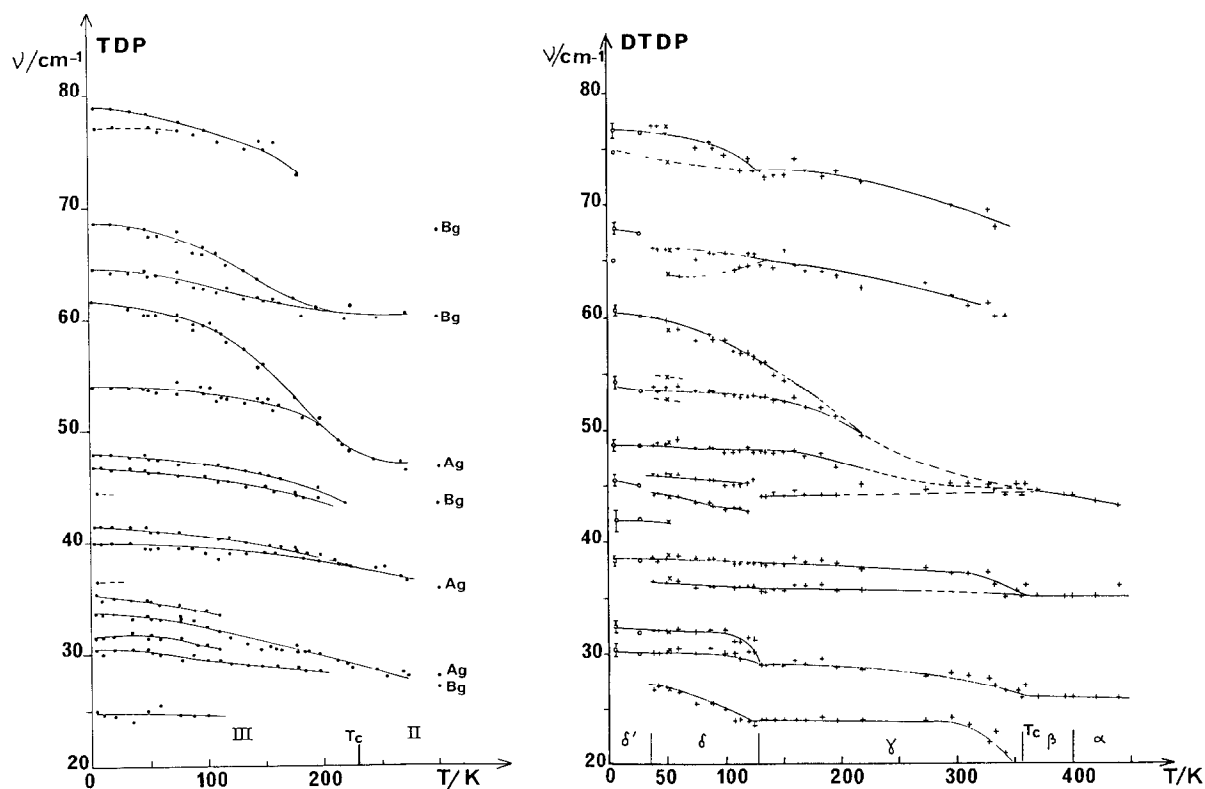


Fig. 3. Temperature dependence of the Raman frequencies for TIH_2PO_4 (TDP) and TID_2PO_4 (DTDP). The lines are guides for the eye.

decomposition if the samples almost fill the sealed containers, in agreement with the results of Zhigarnovskii [24]. Infrared and Raman spectra obtained at 300 K before and after the melting are identical.

5. Vibrational analysis

The proposed assignments are given in tables 1–4. The C_{2h} factor group analysis of the phases II and β predicts 33 external modes due to the H_2PO_4^- entities and the TI^+ ions and 60 internal modes, 36 of them being related to the PO_4 groups and 24 to the hydrogen or deuterium vibrations. In these hydrogen bonded compounds the external modes are usually observed below 300 cm^{-1} .

5.1. External modes

The 33 external modes ($9A_g + 9B_g + 8A_u + 7B_u$)

can be seen as hydrogen-bond stretchings and bendings of the H_2PO_4^- anion sublattice and translational motions of the TI^+ ions against the layers of the hydrogen bonds. According to the $R_{O\dots O}$ distances strong bands due to $\nu_{O\dots O}$ modes are expected above 200 cm^{-1} in the infrared. The $\delta_{O\dots O}$ HB bending may appear in the $100\text{--}50\text{ cm}^{-1}$ range and the TI^+ translational modes are expected below 50 cm^{-1} [26,27]. These spectral ranges are supported by a force-field calculation of the CsH_2PO_4 (CDP) [27]. An isotopic frequency ratio ν_H/ν_D of external modes of about 1.01–1.04 is expected for translational and librational motions respectively. The assignments proposed in table 1 are based on these considerations.

The Raman and infrared (figs. 2 and 4) spectra of phases I, II, α and β present broad features near 200 and 100 cm^{-1} , respectively. They are assigned to the $\nu_{O\dots O}$ and $\delta_{O\dots O}$ HB modes. The strong and narrow Raman bands near 36 cm^{-1} are assigned to the translational TI^+ modes by analogy with the Cs^+ vibra-

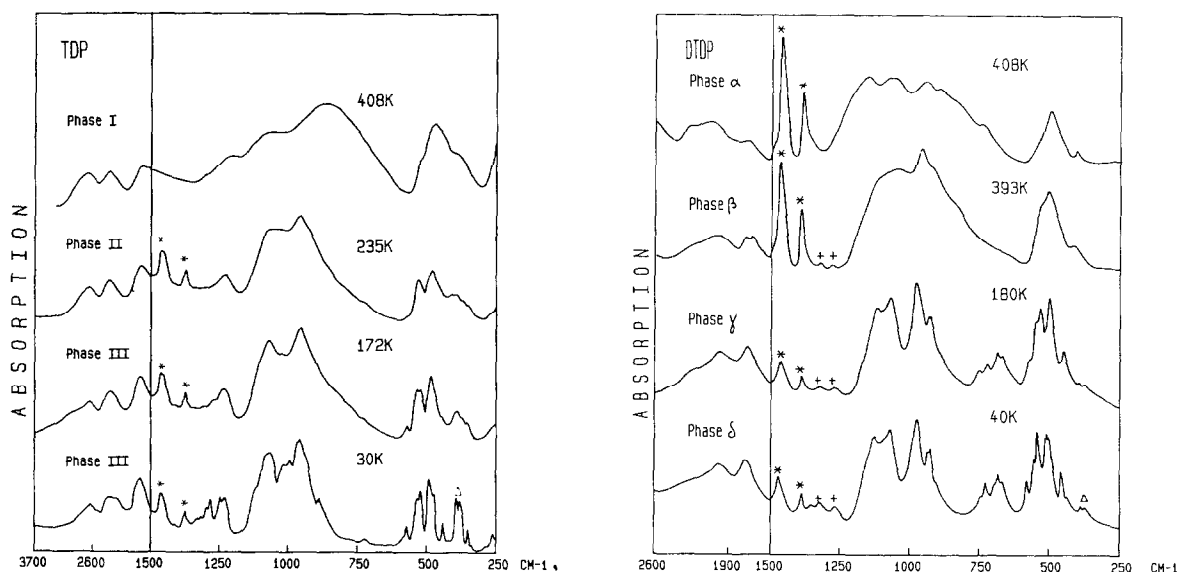


Fig. 4. Infrared absorption spectra for the internal modes of various phases of TiH_2PO_4 (TDP) and TiD_2PO_4 (DTDP). (*) Absorption of Nujol, (+) trace of TDP, (Δ) ν_2 modes of PO_4 groups.

tions in CsH_2PO_4 at 42 cm^{-1} [27]. In fact, the square root of Ti/Cs mass ratio ($= 1.24$) is close to the frequency ratio for the translational modes: $T_{\text{Cs}}/T_{\text{Ti}}$ (≈ 1.20). The great Raman intensity of these bands stems from the high polarizability of the Ti^{1+} ions [28]. According to De Andrès and Prieto [19] polarized infrared and Raman spectra of a single crystal of TDP in phase II show $7A_g + 9B_g + 5A_u + 5B_u$ distinct external-mode frequencies. This is apparently in agreement with the centred group-factor predictions of this disordered crystal. This is in contrast with the internal modes (see below).

No major lattice deformations are expected during the phase transitions (fig. 3). This is consistent with the near-second-order character of the II–III, β – γ and γ – δ transitions revealed by heat-capacity measurements [10,11]. Therefore the assignment schemes for the spectra of phases III and γ , δ and δ' are identical to those of phase II and β . Inelastic neutron-scattering intensities are primarily due to the hydrogen-atom displacements. Comparison of infrared, Raman and INS spectra (fig. 7) of the phase III allows to confirm our previous vibrational assignments. The intense and narrow Raman lines at 42 and 47 cm^{-1} are very weak in the INS. The INS bands near 35 cm^{-1} imply H_2PO_4^- motions.

Below T_c the splitting of many Raman lines is consistent with the doubling of the unit cell. The different components are fully separated only 70 K below T_c . The same temperature dependence of ^{17}O NQR lines has been observed [14]. Moreover, lines between 60 and 50 cm^{-1} in TDP and near 50 and 25 cm^{-1} in DTDP show a pronounced softening in approaching T_c from below and a simultaneous strong decreasing of their maximum intensities. They are assigned to the $\text{O}\cdots\text{O}$ bending modes or/and librational modes of PO_4 groups.

Substantial differences are observed between TDP and DTDP (fig. 8). If the transition II–III is of the paraelectric–antiferroelectric type (as generally proposed [15,16,23]) 36 Raman external modes are anticipated according to the doubling of the centred primitive cell [29] of the phase II. However, 40 lines are distinguished in the Raman spectrum of TDP at 20 K (fig. 7 and table 1). A possible explanation for this greater number of observed bands could be the loss of the inversion centres in phase III. In that case phase III would be ferroelectric as the monoclinic form of RbD_2PO_4 (DRDP) [30,31] rather than antiferroelectric. For DTDP only 33 external modes are distinguished in the Raman spectra of the phase δ . Moreover, a single and strong Raman band is ob-

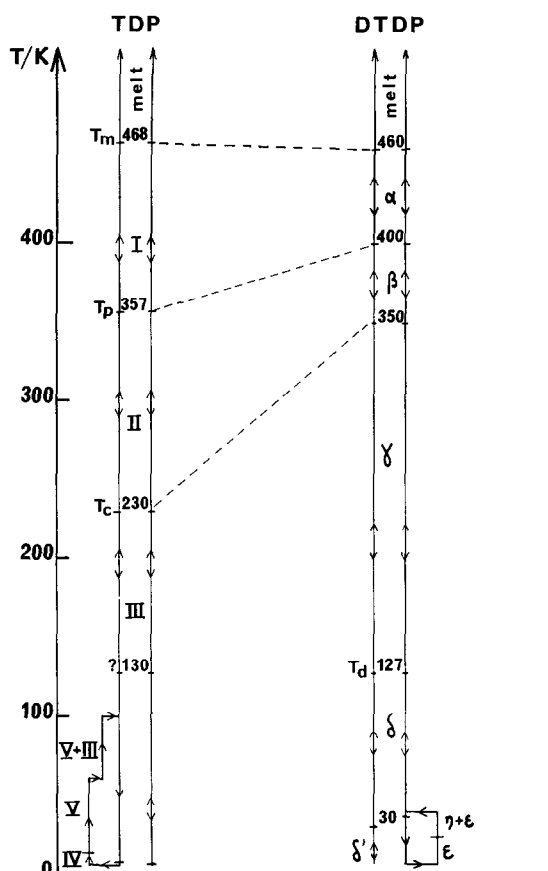


Fig. 5. Phase diagram of TIH_2PO_4 (TDP) and TID_2PO_4 (DTDP) between the melting point and 5 K.

served near 39 cm^{-1} which contrasts to the two bands observed for the translational modes of the cations in TDP (fig. 8). Furthermore the observed values ($\nu_{\text{H}}/\nu_{\text{D}} \leq 1$) for the frequency ratios in the $100\text{--}130\text{ cm}^{-1}$ range differ from the expected values. These facts suggest different hydrogen bonds and different crystal symmetry for TDP and DTDP.

At 6 K the low-frequency Raman spectra of TDP (fig. 2) show only two broad bands at ≈ 95 and $\approx 30\text{ cm}^{-1}$. These frequencies are lower than those corresponding to simple envelopes of the bands of the phase III (≈ 110 and $\approx 45\text{ cm}^{-1}$). Therefore this phase is characterized by a great disorder (band broadening) and less densely packed TI^+ and H_2PO_4^- sublattices.

In phase V the average frequencies for the external bands appear also lower than in phase III. The Ra-

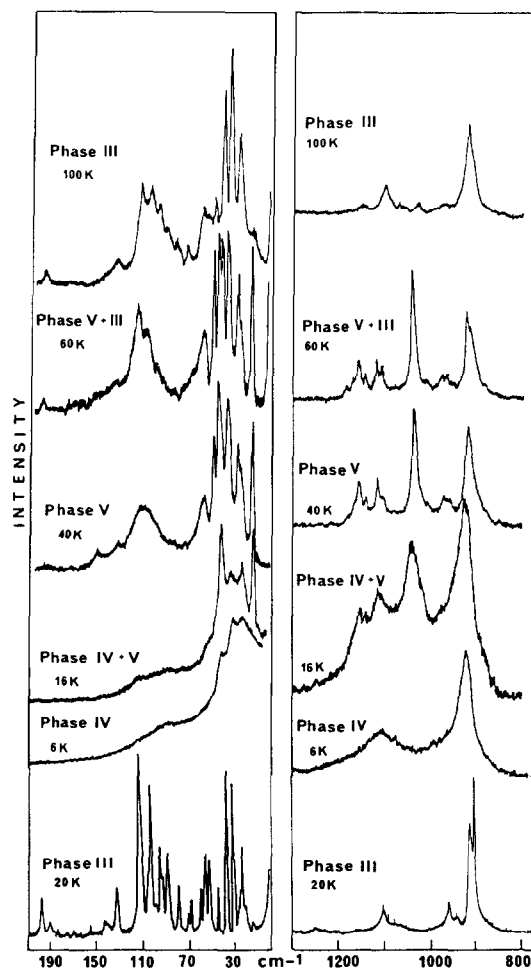


Fig. 6. Evolution of the Raman external and PO_4 stretching modes with the temperature of TIH_2PO_4 . The phase sequence III–IV–V–III is illustrated from bottom to top.

man intensities of both external and internal bands and the bandwidth of hydrogen-bond bending modes near 100 cm^{-1} are also different in phases III and V. The characteristic band near 19 cm^{-1} (fig. 2) shifts to lower frequency in DTDP, and has no soft-mode behaviour. This is assigned to a translational mode involving TI^+ ions and hydrogen-bonded layers. This may reveal a new crystalline structure due to a possible reconstructive transition consistent with the strong disorder of the phase IV.

Table 1

Raman, infrared and inelastic neutron-scattering frequencies (cm^{-1}) of various solid phases of TiH_2PO_4 between 420 and 6 K ^{a)}

I R	II Pol ^{b)}	II		III				IV R	V R ^{d)}	Assignment ^{e)}	
		IR ^{c)}	R	IR ^{c)}	R	IR ^{c)}	R				INS
420 K	300 K	250 K	250 K	180 K	180 K	20 K	20 K	20 K	6 K	40 K	
17vw							24wb			19s 26sh 28sh 31s	T layer-TI
					28		31w				
26m	27Bg 28Ag 30Au		27w		30		32w 34m 35w 37w	35m	30sh	35w	
34s	36Ag 44Bg 46Bu		36s		39		40sh 42s 47s		35s	39s 46sh	T TI-TI
45m	46Ag	40vw	46m	50	51	51w	48vw 54m	≈ 48	48vw 44w	48s 52s	
	52Au 62Bu 62Bg 68Bg 80Bu 85Ag	55m 61w	61w	58	60	61m	61.5s 65.5s 68s 74sh 77m 79w 80m 89w			61m 77w 86w	$\delta_{\text{O-O}}$
	90Au	89sb		95	≈ 93	100m	99w 101.5s 105w 109vs 111w	95m	95mb		
92mb 100sh	97Bg 105Ag		100mb 110sh		104		116w 131m 129w 138m 146w 148w 161w	117m 130w		113mb 134w 152w	T, R PO_4
	130Bu 132Bg	130vw	135sh	≈ 130	135		170m 180w 192m	135sh			
	150Au	150sh		146	146	149m	178w 192w 199m 205m 210vw 221w	146w	158vw	174w	
	175Bg		175sh	166		198	192w 199m 205m 210vw 221w	177m 191m 197sh	197sh	198w 215w	
	195Bu	200sb		200		220	227m 236w 230sh 230w			239w 253w	
228vw	207Au 237Ag 242Ag 242Bg 272Bg		236vw	220	220	227sb	227m 236w 240sh 240m 240m 257w 271m 277w 290w	230w		290sh 295m	$\nu_{\text{O-O}}$

^{a)} Intensity: s, strong; m, medium; w, weak; v, very; b, broad; sh, shoulder.^{b)} Light polarized infrared and Raman spectra.^{c)} Frequency range below 25 cm^{-1} not explored.^{d)} Characteristic spectral features of this phase are shown in italics.^{e)} Translational (T) and librational (R) modes; ($\nu_{\text{O-O}}$) stretching and ($\delta_{\text{O-O}}$) bending modes of the hydrogen bonds (HB) are issued from T, R of PO_4 groups.

Table 2
Raman and infrared frequencies (cm^{-1}) assigned to lattice modes of phases of TlD_2PO_4 between 420 and 6 K ^{a)}

α R	β		γ		δ		δ R ^{d)}	δ R	Assignment
	IR ^{c)} 380 K	R 373 K	IR ^{c)} 155 K	R 157 K	IR ^{c)} 30 K	R 52 K			
16vw							16vw	12vw	} T layer-Tl
				24s			25sh		
							27s		
27w		26sh		29s			30.5w	30sh	} T Tl-Tl
							32s	32.5s	
								23sh	
35s		35vs	40sh	36sh	240sh		36sh	38.5s	} T Tl-Tl
				38vs			39vs	42sh	
				44s			44.5m	45.5m	
42mb		44m		48m			46m	48m	} $\delta_{\text{o.o}}$
				52.5m	53sh		49m	54m	
				55sh			53m	55w	
			54m	61sh	57m		59m	61s	} $\delta_{\text{o.o}}$
							64sh	65sh	
							66s	68w	
		62sh		65s	78s		76wb	75sh	} $\delta_{\text{o.o}}$
				73wb				77m	
	73mb		80sb		82s		85sh	86.5m	
88mb	89sh	93s	95m	86wb	97m		91sh	98vs	} T, R PO_4
				95s			97s	95s	
							101sh		
100shb		105shb		105s			106sh	104s	} T, R PO_4
							108.5m	108s	
							112sh	110sh	
			112w	110s	116w		114.5s	114vs	} $\nu_{\text{o.o}}$
				121s			123s	123.5vs	
		130sh	134sh	135sh	135sh		138m	139m	
			146.5s	147w	149s		143sh	146sh	} $\nu_{\text{o.o}}$
			167sh	170vw	170wb		151w		
			190s		191.5s		171wb	175wb	
	190svb			196m	196sh		175wb	175wb	} $\nu_{\text{o.o}}$
		185vw		196m	196sh		196.5m	198m	
		220wb	220s	224m	225s		226m	227m	
216vw			245shb	232m	234w		235.5m	236m	} $\nu_{\text{o.o}}$
					248s				
				267vw	252sh		275w	273vw	

For footnotes see table 1.

5.2. PO_4 group vibrations

Internal-mode frequencies and assignments in terms of group vibrations are given in tables 3 and 4 for the various phases of both compounds. The four normal modes of a regular tetrahedral PO_4 group, the

stretching ν_3 (F_2) and ν_1 (A_1) and the bending ν_4 (F_2) and ν_2 (E), occur in the 1150–800 and 550–330 cm^{-1} ranges, respectively [32]. In phases II and β four compounds (A_g, B_g, A_u, B_u) are expected for each of the nine normal vibrations of the asymmetric phosphate groups. At 300 K these components can be

Table 3 (continued)

I		II		III		IV	V	Assignment ^{e)}	
IR ^{b)}	R	IR	R	IR	R ^{e)}	R ^{b)}	R ^{b,d)}		
408 K	378 K	250 K	250 K	20 K	20 K	10 K	40 K		
<i>860svb</i>		960s		956vs 965sh		962vs		} $\gamma_{\text{OH}}\text{HB}_2, \text{HB}_3$	
				1220sh 1230m 1246m	1225vw 1243w	1240s			} $\gamma_{\text{OH}}\text{HB}_1$
1220w	1225w	1230m	1250w	1283m 1295m 1313w 1328w	1285w	1304s	1190w	1215vw	
		Nujol		Nujol		1335m			} $\delta_{\text{OH}}\text{HB}_1$
<i>1530mb</i>		νPO_4		νPO_4	920wb	1050sb			
					1080wb				
1650mb	1730wb	1680sb	1700wb 1850sh	1600sh 1700sb 1800sh	1580wb 1700sh 1900sh	1700sh 1820mb		1600w 1970w	} $\nu_{\text{OH}}\text{HB}_2, \text{HB}_3$
2130sh				2160sh	2150shb		2170wb		
2280mb	2300wb	2290sb	2300w	2280sb 2580sh	2300wb	2230mb 2500m		2290w	
2680mb 2840sh	2700wb	2670mb	2700w	2660sb 2720sh	2650w	2650mb		2750w	

^{a)} See footnote a) of table 1.

^{b)} Characteristic spectral features of phase I and phases IV and V relatively to the phases II and III are shown in italics.

^{c)} Brackets: characteristic fwhh of bands.

^{d)} *, **: Frequencies observed at 60, 10 K, respectively.

^{e)} ν_1, ν_3 and ν_4, ν_2 : stretching and bending modes of a regular tetrahedral PO_4 ; HB_1, HB_2 and HB_3 : the three different hydrogen bonds defined in the crystallographic data section.

resolved only using polarized light with a single crystal. Below T_c there are at least eight components.

Fig. 9 shows $5A_g, 5B_g, 3A_u$ and $4B_u$ components in the ν_4 spectral region with some coincident u–g frequencies while $3A_g + 3B_g + 3A_u + 3B_u$ are expected. This suggests that the selection rules related to the inversion centre symmetry of the hydrogen bonds are relaxed. A similar effect has been observed in CDP [27]. Similarly in KDP [4] the spectra disagree with the selection rules anticipated from the site-symmetry (S_4) given by the crystallographic data [5]. Therefore, there is no centre of inversion for the hydrogen bonds on the time-scale of these frequencies.

In the same way, the PO_4 site-symmetry in the orthorhombic phase I is C_1 as in phase II. The spectra of phase I do not show the two intense Raman bands observed in solution for the stretching-modes of a C_2 (or C_s) PO_4 group.

In the Raman spectra of TDP, two systems of bands with different bandwidths (≈ 3 and $\approx 10 \text{ cm}^{-1}$ at 20 K, respectively) can be observed below T_c (table 3, fig. 10). These are related to the existence of two kinds of PO_4 groups. The broadest bands must be due to the PO_4 groups linked by the shortest hydrogen bond (HB_1) and the others to those engaged in the longer hydrogen bond (HB_2). As opposed to these obser-

Table 4

Raman and infrared frequencies (cm^{-1}) assigned to internal modes of the various solid phases of TlD_2PO_4 between 420 and 6 K ^{a)}

α		β		γ		δ		ϵ	Assignment ^{d)}
IR ^{b)} 408 K	R ^{c)} 420 K	IR 393 K	R 373 K	IR 180 K	R 157 K	IR 40 K	R 52 K	R 10 K	
			334sh		332m		313vw 332m	333m	} ν_2
	357m		358s	340vw 363w	361.5s 370sh	340w 360w	336sh 362s 368w	360s	
380w		375wb		390sh 410sh 427m	378w	390w 413vw 430m	378m 415vw 454m	375w 420vw	
	440wb		451mb		462m		459s 470sh	455mb	
490s	486wb	485s	486w	475sh 485s 500w 510w	472m 487s 511m	475m 485s 510s	476s 489s 500w 510m 514sh	470wb 486m 506wb	} ν_4
520sh		515m		525m		525s	521vw 532m	532m	
	538mb		536s	545w	533m 542sh 548m	545m	540w 551m 556sh	546m	
			780vw 843sh		775vw 845m		776vw 845m	775vw 843w	} $\nu_2 + \nu_4$
870shb	885s		886vs	870sh	882vs	875sh	882vs	881vs	} $\nu_1 + \delta_{\text{OD}}$
	906s	886sh	909vs	903m 913w	900sh 911s	900w 915w	902m 912s	904sb	
940s		941s		953s	932wb 945sh		938m 948w 962w	934sh	} ν_3
	1000mb		1000sb		1000vsb		998vsb	996sb	$\delta_{\text{OD}} + \nu_1$
1050s		1052sb		1047sb 1065sh	1050sh 1087sh	1050vsb sh	1050wb 1084mb	1050vw	} ν_3
1150s	1140w	1100sb	1100mb	1100vs	1110vs	1100vs	1093sh 1109s	1090shb 1107s	
650shb		640wb 650shb	658vwb	645m 660m 695m 720w	643w 690w 714vw	645m 662m 697m	615vw 640w 656w 698vw 717vw	640vw	} ν_{OD}
1740m vb		1680m	1720w	1725s	1740w	1720s	1745w	1600sh	} ν_{OD}
2085m vb		2040mb	2020w	1990sb	2015w	1980sb	1998w	2100w vb	
2270m vb		2290sh		2270sh		2250sh			

^{a)} See footnote a) of table 1.^{b)} Characteristic features of phase α relatively to phase β are shown in italics.^{c)} Raman spectra of the ν_{OD} range were not explored.^{d)} ν_1, ν_3 and ν_2, ν_4 : stretching and bending modes of a regular tetrahedral PO_4 .

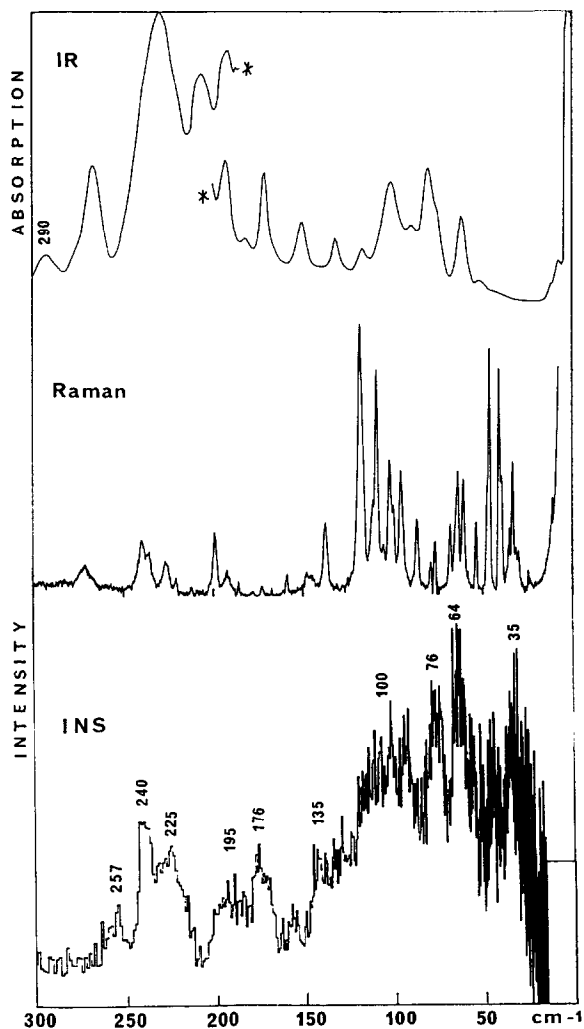


Fig. 7. Infrared, Raman and inelastic neutron-scattering spectra of phase III of TiH_2PO_4 at 20 K (external modes).

vations, no different widths are evidenced in the Raman spectra of DTDP. Moreover, in the infrared the absorptions near 350 cm^{-1} , assigned to the ν_2 modes, are much weaker for DTDP than for TDP (fig. 4). If the site-symmetry group is closed to C_{2v} , these bending modes belong to the infrared-inactive A_2 species and they should be rather weak. A C_{2v} symmetry means that the hydrogen bonds of the D_2PO_4^- anions are equivalent. Therefore the various hydrogen bonds are likely to be more similar in DTDP than in TDP. This is in agreement with the observed bandwidths and the low-frequency spectra.

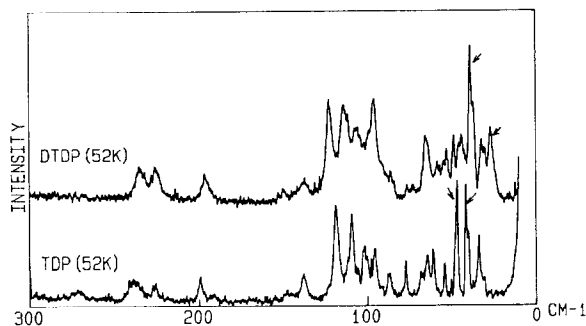


Fig. 8. Comparison of the low-frequency Raman spectra of phases III of TiH_2PO_4 and δ of TiD_2PO_4 at the same temperature.

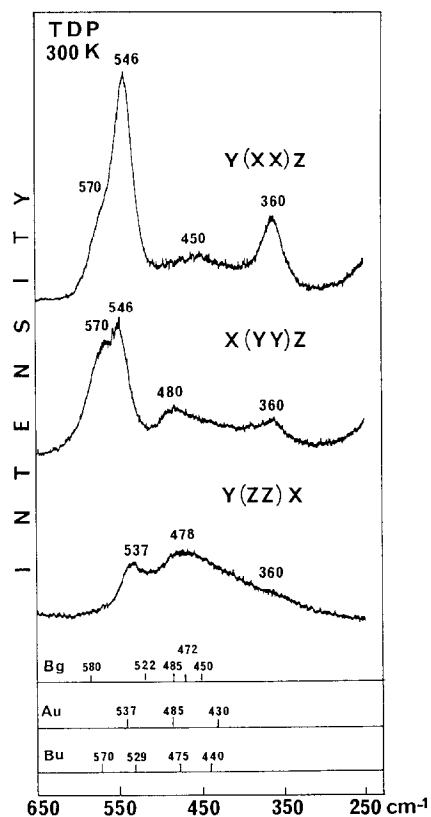


Fig. 9. Raman spectra of ν_2 and ν_4 modes of PO_4 groups of TiH_2PO_4 at room temperature (A_g geometry). B_g , A_u and B_u frequencies of the ν_4 modes are shown as vertical lines.

Relatively to phase III, new Raman lines appear in phase V at 1154 (medium), 1032 and 930 (very strong), 700 (weak) and around 300 cm^{-1} (me-

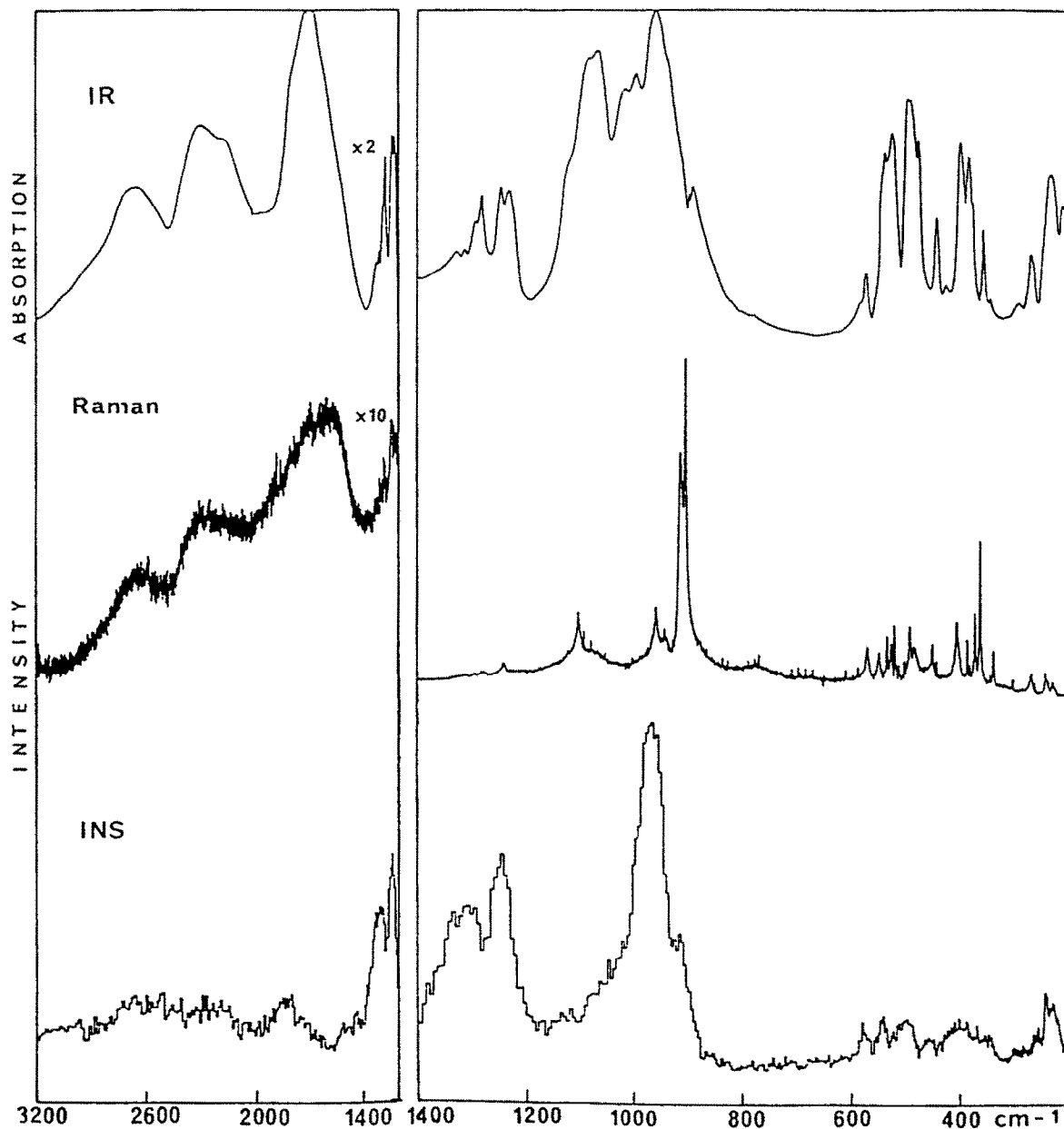


Fig. 10. Infrared, Raman and inelastic neutron-scattering spectra of TiH_2PO_4 at 20 K (internal modes).

dium). It is difficult to explain this new spectrum without any structural information and infrared data. Nevertheless, a proton transfer inside the very short hydrogen bond (HB_1) and the existence of H_3PO_4 and HPO_4^{2-} species are suspected. Indeed Raman spectra of PO_4 group in PbHPO_4 show important

bands near 1040, 934 and 310 cm^{-1} , assigned to the ν_3 , ν_1 and ν_2 modes [33]. The aqueous solution of H_3PO_4 gives rise to an intense Raman line at 1165 cm^{-1} [32], similar to the band at 1154 cm^{-1} in phase V. The presence of different species would account for the bandwidth at $\approx 100\text{ cm}^{-1}$. The extra line at

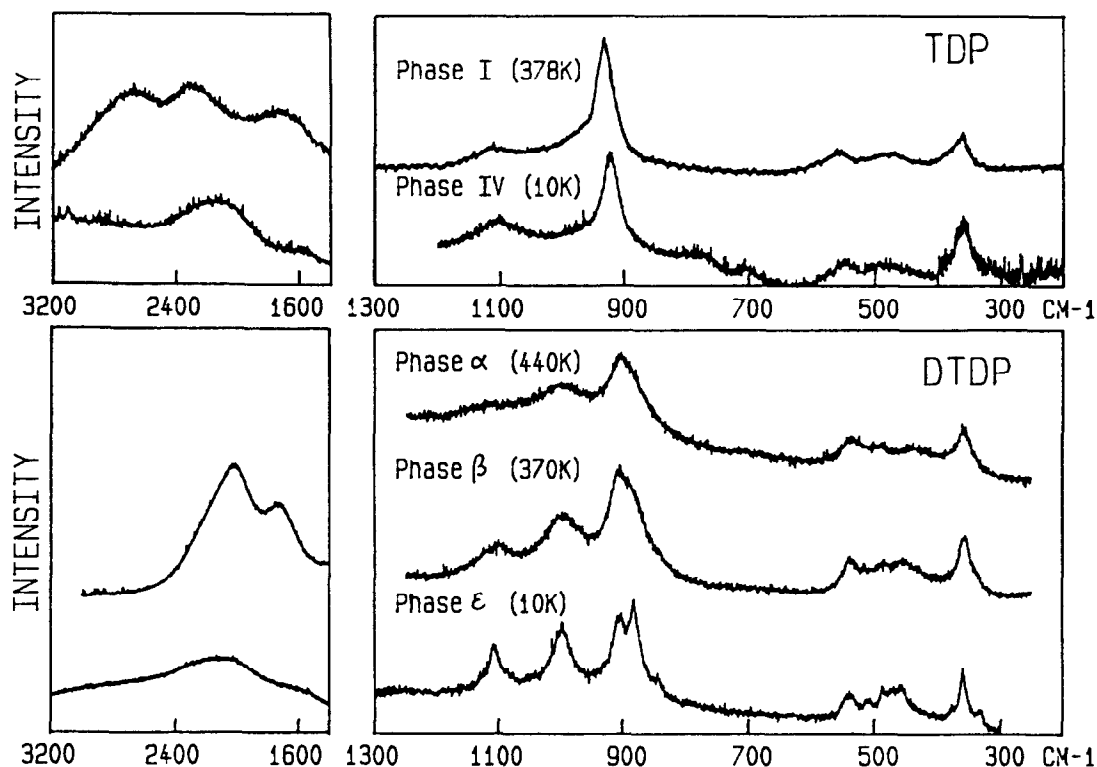


Fig. 11. Comparison of the Raman spectra of disordered low-temperature phases (IV and ϵ) with the high-temperature phases (I and α) (internal modes).

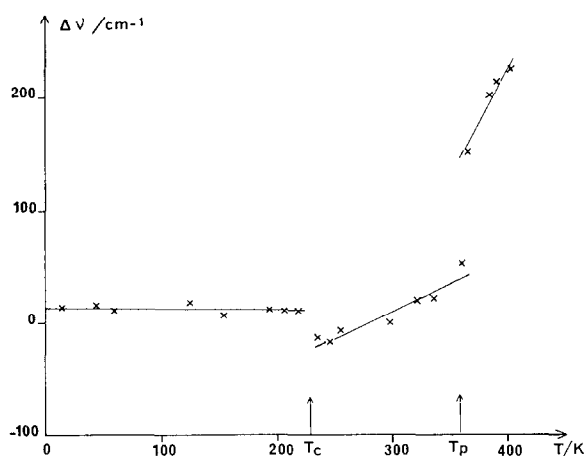


Fig. 12. Temperature dependence of the centre of gravity ν_g of the ABC infrared bands of the OH stretching mode. $\Delta\nu = \nu_g^T - \nu_g^{300\text{K}}$.

700 cm^{-1} , observed in the molten compound and in phase IV, could be a reminiscence of the highly disordered phase IV.

The Raman spectra of the unstable phase IV (6 K) and of the high-temperature phase I (378 K) are quite similar (table 3 and fig. 11). As for the external modes the PO_4 modes reveal a strong disorder in phase IV.

5.3. OH (OD) vibrations

The infrared and Raman spectra of phases I, II and III show a typical “ABC” profile, and in the $1400\text{--}3000\text{ cm}^{-1}$ range, due to the ν_{OH} stretching modes (figs. 4 and 11) of the HB_2 and HB_3 . This is anticipated [26,34] from their O...O distances [22]. A broad band observed near 1050 cm^{-1} in the INS and Raman spectra of TDP at 20 K (fig. 10) may correspond to the ν_{OH} mode of the HB_1 in agreement with the existence of a very short hydrogen bond [26,34] in TDP. This band is hidden in the infrared spectra

by the absorption of ν_3 modes of the PO_4 groups.

The typical ABC profile of the OH stretching mode has been explained by strong mechanical and electrical couplings between the fast ν_{OH} and the slow $\nu_{\text{O-O}}$ modes [35]. This profile does not change significantly upon cooling down through T_p and T_c . However, a plot of the frequency at the centre of gravity of this ABC profile against temperature (fig. 12) reveals two discontinuities at T_c and T_p . This suggests a critical behaviour of the protons at the order–disorder transitions.

The two broad bands between 1400 and 2600 cm^{-1} (fig. 4) in the infrared spectra of DTDP correspond to the OD stretching modes. The frequency at the centre of gravity of these bands appears also sensitive to the T_p and T_c phase transitions as in the case of TDP. However there is no discontinuity for the order–order transition at T_d [20].

The assignment of the δ_{OH} and γ_{OH} modes of the two types of OH vibrators is based primarily on the INS intensities [35,36] (fig. 10) and is given in table 3. The δ_{OD} modes occur in the 1000–900 cm^{-1} range. Their rather strong Raman intensity stems from the coupling with the ν_1 mode of the PO_4 group [27,37] (table 4). In phase I the infrared spectra show two additional absorption bands near 1500 and 860 cm^{-1} (fig. 4) which are assigned to the ν_{OH} of HB_1 and to the γ_{OH} of HB_2 and HB_3 , respectively. All the observations indicate a weakening of the three hydrogen bonds in phase I.

The Raman spectra of phases IV and ϵ show single broad ν_{OH} and ν_{OD} lines (fig. 11) instead of the typical ABC profiles. However the frequency at the centre of gravity of the lines does not increase significantly. These changes of profiles suppose an important change of the dynamical and electrical couplings between the fast ν_{OH} and the slow $\nu_{\text{O-O}}$ modes.

6. Concluding remarks

The analysis presented above allows to draw conclusions concerning the structural features of the various crystalline phases, the characteristics of their transitions and on the proton dynamics in the TiH_2PO_4 (TDP) and TiD_2PO_4 (DTDP) crystals.

Firstly, there are structural differences between TDP and DTDP. In TDP the existence at any tem-

perature of one very short and two longer hydrogen bonds is in agreement with the diffraction data at room temperature [22]. The hydrogen bonds in the deuterated compound appear much less different.

The symmetry or the number of crystallographic sites for the Ti^+ ions seem also different in TDP and DTDP. At low temperature, phase III of TDP appears non-centrosymmetric whilst the phase γ of DTDP is centrosymmetric below T_c . This phase is antiferroelectric. The spectra in phases δ and III suggest that the phase diagrams below T_c are different for TDP and DTDP (temperature domains and crystal symmetry). Different crystal structures and physical properties have already been observed for the hydrogenated and highly deuterated derivatives of KH_2PO_4 [38], RbH_2PO_4 [30,39,40], NH_4HSeO_4 [41,42], RbHSeO_4 [43].

There is however some ambiguity concerning a possible phase transition near 130 K in TDP. This transition could be of nearly second order and similar to the transition observed at 127 K in DTDP. If this transition is real, the same phase diagram would seem to exist for TDP and DTDP and both compounds should be antiferroelectric above ≈ 130 K and ferroelectric below this temperature. The smaller number of bands in phase δ relatively to phase III could be due to more similar hydrogen bonds in the deuterated compound compared to the hydrogenated one. In addition no isotopic effect is expected for T_d which corresponds to an order–order transition.

The occurrence at 10 K of a highly disordered and unstable phase could be the precursor of a new ordered phase at lower temperature. This is supported by the conclusions of Yasuda et al. [44] who estimated the tricritical Curie point at a pressure lower than one atmosphere. Therefore phase IV could be an electric polar glass between phase III and this possible new phase at low temperature. The observation of this disordered phase at low temperature could be related to the ability of TDP to syncrystallize with various compounds [9,28,45,46]. This is a consequence of the large variation of the Ti^+ ionic radius with the host network [47]. Phase V which is obtained from the disordered state and which is also stable at higher temperature does not correspond to this unknown phase.

Secondly the “order–disorder” transitions at T_c

have a clear first-order “displacive” character. This is revealed by the frequency shift of the PO_4 librations in the $60\text{--}50\text{ cm}^{-1}$ frequency range. The Curie transition is likely to be monitored by the reorientation of the PO_4 entities. This is in line with the mechanism which has been proposed for the para-ferroelectric phase transition in KDP [3]. In addition, the absence of soft mode or central mode in TDP favors the “proton partial tunnelling” model [48] which accounts for an order–disorder transition. It is interesting to note that the importance of these reorientations is clearly evidenced in TDP and DTDP where the Ti^+ translations and the hydrogen bond modes are well separated. This is a consequence of the great mass of the Ti^+ ion. The observed frequencies show that the dynamics of the Ti^+ ions are almost unaffected by the phase transition at T_c .

Finally the vibrational analysis in terms of local symmetry of a single crystal in the paraelectric phase II reveals the off-centre localization of protons in the formally centrosymmetric HB_1 and HB_2 hydrogen bonds. The same conclusion applies for the HB_3 hydrogen bonds in the orthorhombic phase I. Therefore TDP is another example where there is no instantaneous symmetry element on the time scale of the internal modes for the hydrogen bonds above T_c . The crystallographic centres of inversion assumed from diffraction studies would then be due to statistical disorder.

Above T_c the vibrational spectra of TDP and DTDP are in agreement with proton ordering in the hydrogen bond. According to this interpretation the discontinuities at T_c and T_p in the OH stretching-frequency curves can be explained by a change in the electrical couplings between the fast ν_{OH} and the slow $\nu_{\text{O}\dots\text{O}}$ modes. This supposes a critical behaviour for the electric field at the order–disorder transitions.

Acknowledgement

The authors wish to thank Dr. A. Novak for critical reading of the manuscript.

References

- [1] Z. Tun, R.J. Nelmes, W.F. Kuhs and R.F.D. Stanfield, *J. Phys. C* 21 (1988) 245.
- [2] R.B. Blinc and B. Žekš, *Ferroelectrics* 72 (1987) 193, and references therein.
- [3] M. Tokunaga and T. Matsubara, *Ferroelectrics* 72 (1987) 175, and references therein.
- [4] M. Tokunaga, Y. Tominaga and I. Tatsuzaki, *Ferroelectrics* 63 (1985) 171; M. Kasahara, K. Motida and M. Ichikawa, *J. Phys. Soc. Japan* 59 (1990) 2600.
- [5] G.E. Bacon and R.S. Pease, *Proc. Roy. Soc. A* 230 (1955) 359; R. Wyckoff, *Crystal structures*, Vol. 3, 2nd Ed. (Interscience, New York, 1963); *International tables for X-ray crystallography*, Vol. 1, 2nd Ed. (The Kynoch Press, Birmingham, 1965).
- [6] M. Ichikawa, *Acta Cryst. B* 34 (1978) 2074; *Chem. Phys. Letters* 79 (1981) 583.
- [7] S. Tanaka, *Phys. Rev. B* 42 (1990) 10488.
- [8] M.I. McMahon, R.J. Nelmes, W.F. Kuhs, R. Dorwarth, R.O. Piltz and Z. Tun, *Nature* 348 (1990) 317.
- [9] H. Sakashita, S. Hayase and H. Terauchi, *Japan. J. Appl. Phys.* 24 (1985) 963.
- [10] T. Matsuo and H. Suga, *Solid State Commun.* 21 (1977) 923.
- [11] J. Bousquet, M. Diot, A. Tranquard, G. Coffy and J.R. Vignalou, *J. Chem. Thermodyn.* 10 (1978) 779.
- [12] H. Yoshida, M. Endo, T. Kaneko, T. Osaka and Y. Makita, *J. Phys. Soc. Japan* 53 (1984) 910.
- [13] R. Mizeris, J. Grigas, R.N.P. Choudhary and T.V. Narasaiah, *Phys. Stat. Sol. (a)* 113 (1989) 597.
- [14] J. Seliger, V. Zagar, R. Blinc and V.H. Schmidt, *J. Chem. Phys.* 88 (1988) 3260.
- [15] J.R. Vignalou, A. Tranquard, M. Couzi and P.V. Huong, *Proceedings of the Fifth International Conference on Raman Spectroscopy*, Freiburg, 1976, p. 594; P.V. Huong, M. Couzi, J.R. Vignalou and A. Tranquard, *Proceedings of the Third Conference on Light Scattering in Solids*, 1975 (Balkanski, Paris, 1975) p. 845.
- [16] N. Yasuda, S. Fujimoto and T. Asano, *Phys. Letters A* 76 (1980) 174.
- [17] Y. Oddon, A. Tranquard and G. Pepe, *Acta Cryst. B* 35 (1979) 542.
- [18] M. Arai, T. Yagi, A. Sakai, M. Komukae, T. Osaka and Y. Makita, *J. Phys. Soc. Japan* 59 (1990) 1285.
- [19] A. De Andrès and C. Prieto, *Phase Transitions* 14 (1989) 3.
- [20] S. Al Homsî-Teiar, Thèse de Doctorat, Université de Paris-VI (1990); B. Pasquier, N. Le Calvé, S. Al Homsî-Teiar and F. Fillaux, *Dismos II* (Garchy, France, 1991).
- [21] P. Simon, F. Gervais and E. Courtens, *Phys. Rev. B* 37 (1988) 1969.
- [22] R.J. Nelmes and R.N.P. Choudhary, *Solid State Commun.* 38 (1981) 321.
- [23] R.J. Nelmes, *Solid State Commun.* 39 (1981) 741.
- [24] B.M. Zhirgarnovskii, Yu.A. Polyakov, K. Rakhimov, V.I. Bukagov, V.Yu. Kozhenov and M.A. Maifat, *Inorg. Mater.* 21 (1986) 1572.

- [25] Y. Oddon, J.R. Vignalou, G. Coffy and A. Tranquard, *Bull. Soc. Chim. France* (1976) 334.
- [26] A. Novak, *Struct. Bonding* 18 (1974) 177.
- [27] B. Marchon, Thèse de Doctorat d'Etat, Université de Paris-VI (1983);
B. Marchon and A. Novak, *J. Chem. Phys.* 78 (1983) 2105.
- [28] B. Matthias, W. Merz and P. Scherrer, *Helv. Phys. Acta* 20 (1947) 18;
J.R. Tessman, A.H. Kahn and W. Shockley, *Phys. Rev.* 92 (1953) 890.
- [29] R. Blinc and B. Žekš, *Selected topics in solid state physics*, Vol. 13. *Soft modes in ferroelectrics and antiferroelectrics* (North-Holland, Amsterdam, 1974).
- [30] S. Suzuki, K. Arai, M. Sumita and Y. Makita, *J. Phys. Soc. Japan* 52 (1983) 2394.
- [31] T. Osaka, M. Sumita and Y. Makita, *J. Phys. Soc. Japan* 52 (1983) 1124.
- [32] A.C. Chapman, D.A. Long and D.T.L. Jones, *Spectrochim. Acta* 21 (1965) 633.
- [33] N. Ohno and D.J. Lockwood, *J. Chem. Phys.* 83 (1985) 4374.
- [34] N.D. Sokolov, M.V. Vener and V.A. Savel'ev, *J. Mol. Struct.* 222 (1990) 365.
- [35] F. Fillaux, *Chem. Phys.* 74 (1983) 395.
- [36] F. Fillaux, B. Marchon, A. Novak and J. Tomkinson, *Chem. Phys.* 130 (1989) 257.
- [37] E. Anachkova and I. Savatinova, *Phys. Stat. Sol. (b)* 131 (1985) K101.
- [38] N.G. Parsonage and L.A.K. Staveley, *Disorder in crystals* (Clarendon Press, Oxford, 1978) p. 412.
- [39] N.S.J. Kennedy and R.J. Nelves, *J. Phys. C* 13 (1981) 4841.
- [40] T. Hagiwara, K. Itoh, E. Nakamura, M. Komukae and Y. Makita, *Acta Cryst. C* 40 (1984) 718.
- [41] Z. Czaplá, O. Czupinski and L. Sobczyk, *Solid State Commun.* 51 (1984) 309.
- [42] I.P. Aleksandrova, Ph. Colombar, F. Denoyer, N. Le Calvé, A. Novak, B. Pasquier and A. Rozycki, *Phys. Stat. Sol. (a)* 114 (1989) 531.
- [43] Z. Czaplá, L. Sobczyk and J. Mroz, *Phys. Stat. Sol. (a)* 70 (1982) 73.
- [44] N. Yasuda, S. Fujimoto, T. Asano, K. Yoshino and Y. Inuishi, *J. Phys. D* 13 (1980) 85.
- [45] M. Bruzau, *Bull. Soc. Chim. France* (1948) 1177.
- [46] Y. Oddon and A. Tranquard, *C.R. Acad. Sci. Paris C* 289 (1979) 309.
- [47] V.C.G. Trew, *Trans. Faraday Soc.* 32 (1936) 1658.
- [48] N. Kojyo and Y. Onodera, *J. Phys. Soc. Japan* 57 (1988) 439.